68th International Astronautical Congress, Bremen, Germany.

IAC-18,C1,6,2,x45169

Balancing Differential Drag with Coulomb Repulsion in Low Earth Orbit Plasma Wakes

Jordan Maxwell[a], Andrew Harris[b], and Hanspeter Schaub[c]

[a] *Graduate Research Assistant, Department of Aerospace Engineering Sciences, University of Colorado, 431 UCB, Colorado Center for Astrodynamics Research, Boulder, CO 80309-0431*, jordan.maxwell@colorado.edu

[b] *NDSEG Fellow, Department of Aerospace Engineering Sciences, University of Colorado, 431 UCB, Colorado Center for Astrodynamics Research, Boulder, CO 80309-0431*, andrew.harris@colorado.edu

[c] *Glenn L. Murphy Endowed Chair, Department of Aerospace Engineering Sciences, University of Colorado, 431 UCB, Colorado Center for Astrodynamics Research, Boulder, CO 80309-0431*, hanspeter.schaub@colorado.edu

Abstract

A novel method for close-proximity formation flying under differential atmospheric drag using Coulomb forces is investigated for applications in Earth sensing, space-situational awareness (SSA), and aeronomy. Objects in LEO are supersonic with respect to the ambient environment, creating a thinned out wake region antiparallel to the craft's atmosphere-relative velocity. Objects within this wake will experience little drag acceleration and are able to attain voltages much greater than in the ambient ionospheric plasma, creating implications for the design and control of close-proximity leader-follower spacecraft pairs. The proposed system consists of a leader craft with a set of affixed, conducting spheres and a charged follower craft located in the wake of the leader. The differential drag acceleration between the leader and follower craft is countered by a controlled Coulomb repulsion to maintain precise separation. The charge structure on the rear of the leader craft is designed such that the charged follower craft sits in an electrostatic potential well which opposes off-axis perturbations. A conceptual method for controlling such a pair without the use of propellant using a set of charged spheres is investigated, with nonlinear models of the system's relative motion derived and discussed. Linearized models are used to demonstrate the local controllability of the system to demonstrate the proposed system's merit. This linear analysis is used to derive conditions on controllability and control performance under various charge geometries and environmental assumptions.

1. Introduction

Close-proximity formation flying is an enabling technology for next-generation missions involving Space Situational Awareness, spacecraft servicing,[1] debris mitigation, or Earth observation. However, close-proximity formation flight represents a substantial challenge to spacecraft guidance, navigation, and control technologies, especially when tight position constraints are imposed by one of the aforementioned mission types. The use of traditional thrusters for formation-flight control increases mission mass and cost; additionally, thruster plumes for close-proximity flight can cause undesirable effects due to plume impingement on neighboring spacecraft. By fusing concepts from differential-drag formation flight and Coulomb-actuated formation flight, this work aims to demonstrate the feasibility of non-impulsive formation flight that leverages the space environment to achieve tight formation control tolerances.

Traditional approaches to close-proximity formation flight consider the application of impulsive thrusters as actuators. The CanX-4/5 dual spacecraft experiment utilized a pair of nanosatellites to achieve sub-meter level control accuracy while using between 1.15 and 3.4 cm/s of ΔV per orbit.[2] While these values are small, they imply that a multi-year formation flight mission would require hundreds of meters per second of ΔV, which would require steep trade-offs from other mission areas. For these reasons, it is desirable for future high-precision formation flight missions to leverage forces originating from the space environment whenever possible.

The study of environmental forces for formation actuation is substantial. For spacecraft in LEO, drag forces are a dominant perturbation force.[3] Differential drag formation flight, which uses differences in drag forces acting on spacecraft to achieve relative accelerations, has been used to constitute and maintain formations operationally as described by Foster.[4] However, uncertainty in forecasts of atmospheric density[5] and spacecraft drag coefficients,[?] combined with the small magnitude of drag forces, largely prevents their application to the high-precision formation flight domain.

Charging of spacecraft using electron or ion-beams results in Coulomb forces that represent another method of zero-propellant maneuvering for formation flight. First

described by King,[6] Coulomb formation flight is largely considered in the context of GEO formation flight[7] due to the need for low plasma densities to prevent charge dispersion and plasma shielding effects. Multiple studies have demonstrated the controllability of formations where individual spacecraft are considered as charged spheres.[8] The recent development of Multi Sphere Method[9] (MSM) has allowed for the consideration of dynamics between two spacecraft represented as collections of charged spheres, enabling considerably more complex dynamics. The presence of relatively dense ambient plasmas in LEO prevents extreme spacecraft charging by providing a medium for charge transfer, and as a result few studies in the use of Coulomb actuation for LEO formation flight have been undertaken. Additionally, the Debye length in LEO plasma is on the order of 1cm, so electrostatic forces and torques are attentuated significantly beyond this distance. However, recent studies in the dynamics of spacecraft plasma wakes — regions of decreased plasma density produced behind spacecraft as they move through space–suggests that GEO-like plasma environments exist "behind" spacecraft in LEO.[10] Additionally, the reduced density of plasma and neutral species in the wake reduces drag forces acting on spacecraft in the wake, creating relative accelerations due to differential drag. This work envisions a formation flight system that leverages the unique physics of the wake by applying Coulomb repulsion to balance differential drag effects and thereby enable high-precision, close-proximity formation flight in LEO.

This work is arranged as follows. First, the architecture of the proposed formation flight system is presented alongside bounding assumptions. Next, the non-linear dynamics of such a system are derived from first principles. These dynamics are then linearized about an equilibrium condition that uses Coulomb repulsion to counter-act drag forces acting on the leader spacecraft. The linear controllability of this system is examined for a variety of feasible system parameters and assumed drag accelerations. Finally, a representative, controlled system is demonstrated using the true non-linear dynamics under additional non-modeled perturbations to validate this approach.

2. Problem Statement

A two-spacecraft, along-track formation in Low Earth Orbit (LEO) is considered in this work, which aims to study the feasibility of coulomb-balanced differential-drag formation flight in LEO spacecraft wakes. Prior studies in DPCA mission design have shown a required baseline offset on the order of meters, with this relative rectilinear position being held to sub-centimeter accuracy. These parameters are considered as bounding constraints to inform the parameters considered by this study.

The mission concept is illustrated in Figure 1. A charge structure consisting of n_{cs} spheres at a radius r_{cs} is attached to the back of the leader craft. A charged follower craft is offset in the along-track direction by some distance ρ_{f}. Because the wake exhibits decreased neutral density as well as plasma density, the drag acceleration on the follower is assumed to be zero. Differential drag will always decrease the separation between the leader and follower in this case, so voltages are sourced on the follower and charge structure to cancel the drag acceleration of the leader. Negative voltages are chosen because the wake is only ion devoid — the presence of electrons means that negative voltages will require less power than positive ones. Additionally, shielding of negatively signed potentials in an electron-dominated plasma is significantly less than that of those positive.[11] Therefore, the wake acts as vacuum for negative potentials. Therefore, a "pusher-only" control is used in which the controller only ever sources repulsive Coulomb forces. If the follower exceeds the nominal separation, the voltages are nulled and differential drag brings the craft back together. For this investigation, it is assumed that the tight tolerance on relative position will also require the craft to remain in the wake. MSM is applied to calculate the Coulomb acceleration between the leader and follower crafts.

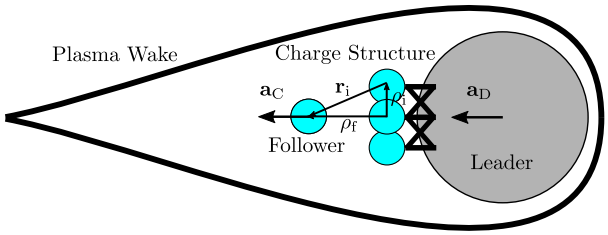

Fig. 1: Illustration of the Coulomb-balanced differential drag concept

3. Nonlinear Equations of Motion

Three perturbations are included in the simplified model used throughout this investigation: Two-body gravity, orbital drag, and Coulomb forces. The Hill frame is used with the origin at the center of the charge structure attached to the leader. Therefore, the accelerations of the follower relative to the leader (stationary in the Hill frame) are used throughout.

$$^{\mathcal{H}}\boldsymbol{\rho} = [\mathcal{NH}]\left(^{\mathcal{N}}\boldsymbol{r}_{\text{f}} - {}^{\mathcal{N}}\boldsymbol{r}_{\text{L}}\right) \tag{1}$$

Henceforth, the left superscript on $\boldsymbol{\rho}$ and its derivatives is suppressed. The state of the system is defined $\boldsymbol{X} = [\boldsymbol{\rho}, \dot{\boldsymbol{\rho}}]^T$ and evolves according to the equation

$$\dot{\boldsymbol{X}} = \boldsymbol{F}(\boldsymbol{X}, \boldsymbol{V}) \tag{2}$$

where $\boldsymbol{F}$ is a non-linear vector function of the state and voltages $\boldsymbol{V}$ which, in this case, incorporates two-body gravity, atmospheric drag, and Coulomb forces.

3.1 Coulomb Acceleration

The Coulomb acceleration of the follower relative to the leader is calculated from the charge on the follower and the electric field of the leader. It is assumed throughout that the large mass of the leader relative to the follower results in a negligible acceleration of the leader resulting from repulsion with the follower.

$$\boldsymbol{F}_{\mathrm{C}}(\boldsymbol{X},\boldsymbol{V}) = \frac{Q_{\mathrm{f}}\boldsymbol{E}_{\mathrm{L}}(\boldsymbol{X},\boldsymbol{V})}{m_{\mathrm{f}}} \tag{3}$$

The proximity of the follower to the charge structure on the leader means that a mutual capacitance exists between the two objects. This affect is described by the relation between the voltage and the charge on a given object.

$$V_i = k_c\frac{Q_i}{R_i} + k_c\sum_{j=1,j\neq i}^{n}\frac{Q_j}{r_{i,j}} \tag{4}$$

where $k_{\mathrm{C}} = 8.99\times10^{9}\mathrm{Nm}^2/\mathrm{C}^2$ is Coulomb's constant, R_i is the radius of the i^{th} sphere, and $r_{i,j}$ is the distance between the i^{th} and j^{th} spheres. Throughout this paper, the subscript 1 refers to the follower and subscripts 2 through n refer to the spheres on the charge structure. The relation above can be rewritten into a single matrix equation.

$$\begin{pmatrix} V_1 \\ V_2 \\ \vdots \\ V_n \end{pmatrix} = k_c \begin{bmatrix} 1/R_1 & 1/r_{1,2} & \dots & 1/r_{1,n} \\ 1/r_{2,1} & 1/R_2 & \dots & 2/r_{2,n} \\ \vdots & \vdots & \ddots & \vdots \\ 1/r_{n,1} & 1/r_{n,2} & \dots & 1/R_n \end{bmatrix} \begin{pmatrix} Q_1 \\ Q_2 \\ \vdots \\ Q_n \end{pmatrix} \tag{5}$$

Written in a more compact fashion

$$\boldsymbol{V} = [S]\boldsymbol{Q} \tag{6}$$

Here, $[S]$ is the elastance matrix. Another, well-known expression relating charge to voltage, $\mathbf{Q} = [C]\mathbf{V}$ indicates that the capacitance is the inverse of the elastance matrix.

$$\mathbf{Q} = [S]^{-1}\mathbf{V} \tag{7}$$

This form is preferable, as the voltage is the control variable and the charge dictates the dynamics. The charge on the follower can be written as an inner product between the first row of the capacitance and the voltage vector. Following the convention establish above, the subscript f from equation (3) is replaced with 1 to indicate the row in the capacitance matrix.

$$Q_{\mathrm{f}} = \boldsymbol{C}_1^T\boldsymbol{V} \tag{8}$$

The electric field from the charge structure $\boldsymbol{E}_{\mathrm{L}}$ at the position of the follower can be calculated by summing the individual fields from each of the spheres on the charge structure.

$$\boldsymbol{E}_L(\boldsymbol{X},\boldsymbol{V}) = k_{\mathrm{C}}\sum_{i=2}^{n}\frac{\boldsymbol{C}_i^T\boldsymbol{V}}{r_{1,i}^3}\boldsymbol{r}_{1,i} \tag{9}$$

Substituting Equations (8) and (9) into (3) yields the non-linear acceleration of the follower subject to the leader.

$$\boldsymbol{F}_{\mathrm{C}}(\boldsymbol{X},\boldsymbol{V}) = \frac{k_{\mathrm{C}}}{m_{\mathrm{f}}}\boldsymbol{C}_1^T\boldsymbol{V}\sum_{i=2}^{n}\frac{\boldsymbol{C}_i^T\boldsymbol{V}}{r_{1,i}^3}\boldsymbol{r}_{1,i} \tag{10}$$

However, an additional complication presents itself. The coupling through the mutual capacitance described by Eq. (5) means that the proximity of two nearby objects affects their charge. To demonstrate this affect, Eq. (8) is expanded.

$$Q_1 = C_1V_1 + \sum_{i=2}^{n}C_{1,i}V_{1,i} \tag{11}$$

As a rule, the self capacitance of an object (C_1) is always positive, while the mutual capacitance ($C_{1,i}$) is always negative. Physically, this results in nearby objects of the same voltage causing a decrease in charge on — in this case — the follower craft. This means that there are sets of voltages and relative positions for which a given Coulomb acceleration cannot be generated. To demonstrate this, consider the mission scenario discussed above and recall that the Coulomb accelerations between the leader and follower are proportional to the charge products.The norm of Eq. (10) is expanded assuming the charge structure spheres are all at the same potential V_2. As discussed previously, the desired Coulomb acceleration is that which perfectly opposes the drag acceleration in the along-track direction.

$$\begin{aligned} |\boldsymbol{F}_{\mathrm{C}}(\boldsymbol{X},\boldsymbol{V})| &\stackrel{!}{=} \\ -a_{\text{Drag}} &= \frac{k_{\mathrm{C}}}{m_{\mathrm{f}}}\left\{\left(C_1V_1 + V_2\sum_{i=2}^{n}C_{1,i}\right)\right. \\ &\left. + \left(V_1\sum_{i=2}^{n}\frac{C_{1,i}}{r_{1,i}^2} + V_2\sum_{i=2,j=2}^{n}\frac{C_{i,j}}{r_{i,j}^2}\right)\right\} \end{aligned} \tag{12}$$

This equation can be re-expressed as a quadratic in V_2, assuming a charge structure voltage is desired to be found for a given follower voltage V_1. The following substitutions are made to simplify the equation. The conditions in this equation recall the discussion of the signs of self and mutual capacitance above.

$$\begin{aligned}\alpha &= C_1 > 0 \\ \beta &= \sum_{i=2}^{n} C_{1,i} < 0 \\ \gamma &= \sum_{i=2}^{n} \frac{C_{1,i}}{r_{1,i}^2} < 0 \\ \delta &= \sum_{i=2,j=2}^{n} \frac{C_{i,j}}{r_{i,j}^2} < 0\end{aligned} \tag{13}$$

Eq. (12) is written as a quadratic

$$0 = \beta\delta V_2^2 + (\alpha\delta + \beta\gamma)V_1V_2 + (\alpha\gamma V_1^2 + a_{\text{Drag}_y}) \tag{14}$$

The condition on real voltages satisfying this expression come from the square root term in the quadratic equation. This condition is written

$$(\alpha\delta + \beta\gamma)^2 V_1^2 - 4\beta\delta(\alpha\gamma V_1^2 + a_{\text{Drag}_y}) > 0 \tag{15}$$

Solving for V_1 yields the final condition for the minimum follower voltage.

$$V_1^2 > \frac{a_{\text{Drag}_y}\beta\delta}{(\alpha\delta - \beta\gamma)^2} \tag{16}$$

Note here that, given the sign of the substituted variables indicated in Eq. (13), there is a minimum follower voltage for all possible configurations.

4. Linearization of Equations of Motion

To apply linear control techniques, Eq. (2) must be linearized about some reference state and potential vector.

$$\dot{\boldsymbol{X}} \approx \boldsymbol{F}(\boldsymbol{X}_0, \boldsymbol{V}_0) + \left.\frac{\partial \boldsymbol{F}}{\partial \boldsymbol{X}}\right|_{\boldsymbol{X}_0} (\boldsymbol{X} - \boldsymbol{X}_0) + \left.\frac{\partial \boldsymbol{F}}{\partial \boldsymbol{V}}\right|_{\boldsymbol{V}_0} (\boldsymbol{V} - \boldsymbol{V}_0) \tag{17}$$

The value $\boldsymbol{F}(X_0, V_0)$ is the derivative of the state at the reference. Moving this term to the left side and using the Δ notation to indicate the different between the variables and their reference values gives the familiar state-space form of the equations.

$$\boldsymbol{\Delta}\dot{\boldsymbol{X}} = \left.\frac{\partial \boldsymbol{F}}{\partial \boldsymbol{X}}\right|_{\boldsymbol{X}_0} \boldsymbol{\Delta X} + \left.\frac{\partial \boldsymbol{F}}{\partial \boldsymbol{V}}\right|_{\boldsymbol{V}_0} \boldsymbol{\Delta V} \tag{18}$$

The linearization of the Coulomb acceleration with respect to the state variable is complicated, as both the relative positions $\boldsymbol{r}_{1,i}$ and the capacitance C depend on the states.

$$\begin{aligned}\frac{\partial \boldsymbol{F}_{\text{C}}}{\partial \boldsymbol{X}} = \frac{k_{\text{C}}}{m_{\text{f}}} \Bigg\{ &\left(\frac{\partial \boldsymbol{C}_1^T}{\partial \boldsymbol{X}}\boldsymbol{V}\right) \sum_{i=2}^{n} \frac{\boldsymbol{C}_i^T \boldsymbol{V}}{r_{1,i}^3} \boldsymbol{r}_{1,i} + \\ &\boldsymbol{C}_1^T \boldsymbol{V} \sum_{i=2}^{n} \Bigg[\frac{\partial \boldsymbol{C}_i^T}{\partial \boldsymbol{X}} \frac{\boldsymbol{V}}{r_{1,i}^3} \boldsymbol{r}_{1,i} + \frac{\partial r_{1,i}^{-3}}{\partial \boldsymbol{X}} \boldsymbol{C}_i^T \boldsymbol{V} \boldsymbol{r}_{1,i} \\ &\frac{\partial \boldsymbol{r}_{1,i}}{\partial \boldsymbol{X}} \frac{\boldsymbol{C}_i^T \boldsymbol{V}}{r_{1,i}^3} \Bigg] \Bigg\}\end{aligned} \tag{19}$$

The derivative of the capacitance is necessarily a $n \times n \times 3$ tensor. Tensors of this shape are henceforth indicated with a bar over the matrix, as shown in Eq (20). Additionally, the prime notation here is used to denote the derivative with respect to the state. The derivative of the capacitance can be calculated by relation to the elastance, for which a simple analytic expression (Equation (5)) exists.

$$\overline{\overline{[C']}} = \frac{\overline{\overline{\partial [C]}}}{\partial \boldsymbol{X}} = -[C]\overline{\overline{[S']}}[C] \tag{20}$$

.

Similar to the usage of capacitance vectors previously, the sub-matrices of the capacitance derivative are denoted $[C_i']$ henceforth.

$$\begin{aligned}\frac{\partial \boldsymbol{F}_{\text{C}}}{\partial \boldsymbol{X}} = \frac{k_{\text{C}}}{m_{\text{f}}} \Bigg\{ &\left(\sum_{i=2}^{n} \frac{\boldsymbol{C}_i^T \boldsymbol{V}}{r_i^3} \boldsymbol{r}_i\right) \left([C_1']^T \boldsymbol{V}\right)^T + \\ &\left(\boldsymbol{C}_1^T \boldsymbol{V}\right) \sum_{i=2}^{n} \frac{[C_i']^T \boldsymbol{V} \boldsymbol{r}_i + \boldsymbol{C}_i^T \boldsymbol{V}([I] - 3\boldsymbol{r}_i \boldsymbol{r}_i^T)}{r_i^3} \Bigg\}\end{aligned} \tag{21}$$

In addition to these accelerations due to the nominal sphere voltages, additional dynamics are present from relative orbital motion with drag. Under the assumptions of a circular leader orbit and nearby follower orbit, the formulation of the Hill-Clohessy-Whiltshire (HCW) equations with linearized drag forces presented first by Silva[12] and modified by Harris[13] is considered. While these equations of motion typically also include a secular differential drag acceleration; however, this acceleration is assumed to be cancelled by the nominal voltage of the follower and charge structure. Using these assumptions, the full system dynamics are produced by summing the state dynamics matrices of the HCW-plus-drag and Coulomb perturbed systems:

$$A_{\text{full}} = A_{\text{HCW+drag}} + \frac{\partial \boldsymbol{F}_C}{\partial \boldsymbol{X}} \tag{22}$$

The linearization of the Coulomb acceleration with respect to the control variable — the voltages on the follower and charge structure — is more straightforward, as the capacitance does not depend on this variable.

Table 1: Minimal controllability summary

Arrangement	Controllable Eigenvectors
Single sphere	In-Plane directions
Two Spheres, In-Plane	In-Plane directions
Two Spheres, Out-of-Plane	All directions

$$B = \frac{\partial \boldsymbol{F}_{\mathrm{C}}}{\partial \boldsymbol{V}} = \frac{k_{\mathrm{C}}}{m_{\mathrm{f}}} \left\{ \left(\sum_{i=2}^{n} \frac{\boldsymbol{C}_i^T \boldsymbol{V}}{r_i^3} \boldsymbol{r}_i \right) \boldsymbol{C}_1^T + (\boldsymbol{C}_1^T \boldsymbol{V}) \sum_{i=2}^{n} \frac{\boldsymbol{r}_i \boldsymbol{C}_i^T}{r_i^3} \right\} \tag{23}$$

The matrices in Eqs. (21) and (23) are evaluated at the nominal follower position and potential vector, respectively, to obtain the linearized dynamics is state space form as shown in Eq. (18).

5. Results & Discussion

5.1 Linear Controllability

Prior to examining linear controllability, the passive dynamics of the system are examined through eigenvalue analysis. Linear controllability can be readily established using the linearized equations of motion by analyzing the column and null space of the controllability matrix M:

$$M = \begin{bmatrix} B & AB & A^2B & \dots & A^nB \end{bmatrix} \tag{24}$$

Prior work on Coulomb-tethered spacecraft and Coulomb-controlled formation flight has suggested several results for this system's controllability.

In a minimal sense, only the in-plane states are found to be controllable with a single sphere on the leader spacecraft. While a single sphere could in theory produce only positive or negative accelerations in the Hill-y direction, controllability is achieved due to in-plane coupling in the HCW equations. Fundamentally, this result grounds the following results by replicating the controllability results found by Natarajan[8,14] with respect to a two-sphere formation actuated only by Coulomb attraction. Notably, due to the assumption of two-body motion, the out-of-plane mode is marginally stable and will remain bounded.

Out-of-plane controllability is achieved with the addition of a second sphere. Because the system has been linearized about an in-plane equilibrium, full controllability could not be achieved if the charge structure is arranged in-plane, i.e. along the Hill x axis. However, a line of charged spheres along the out-of-plane axis yields full controllability in the position and velocity states, as the r_i states gain a component along the out-of-plane axis. These results are summarized in Table 1.

5.2 Control Sensitivity

With the linear controllability of the system established, it is necessary to further examine the sensitivity of prospective controllers to the selection of multiple system parameters. First, pole-placement control was used to specify a system settling time reflecting the half-period perturbation frequency outlined in Section 2. The settling time τ_s of a linear system is taken to be

$$\tau_s = \frac{-4}{\lambda_{\min}} \tag{25}$$

where $\lambda_{\min}$ is the eigenvalue of the feedback-stabilized system $A - BK$ with the smallest magnitude. This approach allows for system designs using different parameters to be examined without sacrificing high-level mission requirements.

A major concern with this approach is the validity of the linearization under large control voltages. As such, the selection of system parameters should minimize the control voltage requested by the controller. In an equivalent sense, it is desirable for changes from the reference voltage to have a large impact on the system's states. For a linear system, the impact of these parameters is governed by the control effect matrix B. For systems that satisfy the necessary conditions for controllability derived in Section 5.1, the Frobenius norm of B is used as an index of control sensitivity with respect to parameter variation:

$$\mathrm{norm}(B) = \sqrt{\sum_{i} = 1^{m} \sum_{j} = 1^{n} |a_{ij}|^2} \tag{26}$$

The sensitivity of B with respect to the follower voltage V_f and the number of spheres constituting the charge structure n was evaluated for a range of plausible values of n and V_f, resulting in Figure 2. The norm of B scales log-logarithmically as V_f increases, as each sphere carries a larger voltage under nominal conditions. At the same time, the norm of B drops as the number of spheres increases, reflecting the fact that attractive and repulsive forces between spheres cancels out some degree of controllability. These results show that the norm of B is largest when the charge structure consists of only a handful of spheres and the follower maintains a relatively large voltage.

Using $n_{\mathrm{cs}} = 2$ and $V_f = 1000V$, the sensitivity of $\mathrm{norm}(B)$ was investigated with respect to the charge structure radius, r_{cs}, and the sphere shell radius as a function of the charge structure side length, $r_i/(2r_{\mathrm{cs}})$. These results are shown in Figure 3. Here, it is apparent that the norm of B increases with both the charge structure radius and the radii of the spheres constituting the charge structure. As the charge structure radius increases, additional control authority is achieved by the larger components of the forces resulting from each sphere along axes other than the Hill y direction. similarly, as the sphere radii increase, the electric field generated by each sphere for a given voltage increases in magnitude, resulting in larger forces on the follower.

From these sweeps, it is apparent that a system designed for maximized control effectiveness will use the

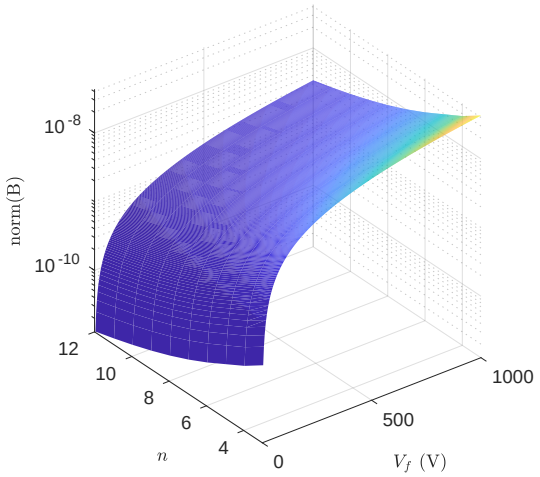

Fig. 2: norm(B) variation with respect to n and V_f.

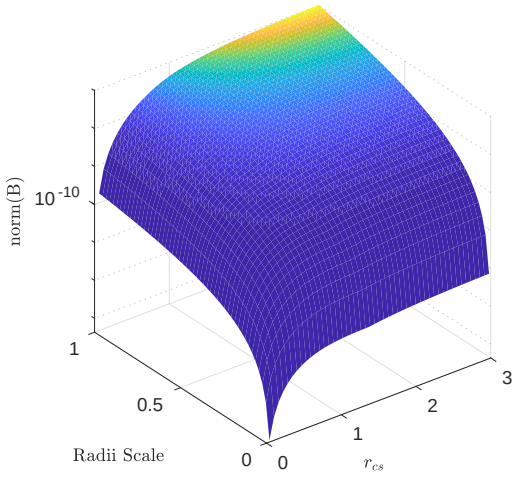

Fig. 3: norm(B) variation with respect to r_{cs} and r_i/r_{cs}.

largest feasible ring of charges, sphere radii, and follower voltage while minimizing the number of spheres used.

5.3 Simulation Results

Simulations are performed applying the linear control law derived above to the nonlinear dynamics in a variety of cases. The controller is run at 0.2Hz and control gains are chosen such that the system settles within ∼45 minutes (0.5 orbits). The orbit elements of the leader are $[6700\text{km}, 0, 0°, 0°, 20°, 0°]^T$. Note that a lower orbit is used so that the leader experiences significant drag. A nominal separation distance of 1m in the along-track direction is chosen to fit the requirements of a DCPA mission.

For direct comparison with the discussion immediately above, an initial simulation is performed applying the parameters outlined in Table 2. Additionally, perfect knowledge of the follower craft's HCW position is assumed. These parameters and assumptions will be changed in later simulations. The mass of the leader is large compared with the follower such that the equal and opposite Coulomb force generated by the voltages on the follower and charge structure results in a small relative acceleration. The performance of the control is considered for a case in which the follower is offset from the nominal position — about which the linearization is performed — by 1cm in the along-track direction.

Table 2: Minimum Control Norm Design Parameters

Parameter	Value
V_{f}	1000V
n_{cs}	2
r_{cs}	3m
r_{s}	2.5m

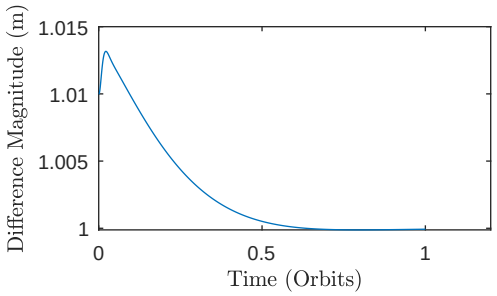

Fig. 4: HCW-frame follower position magnitude for perfect feedback system

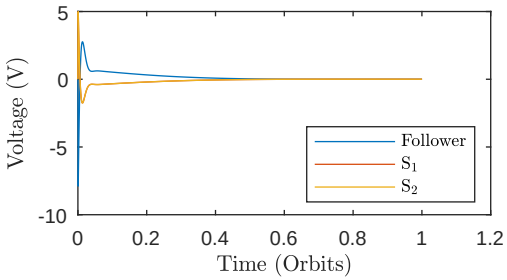

Fig. 5: Control voltage for perfect feedback system. These values are superimposed onto a leader craft at $V_{\text{f}} = -1000V$ and $V_{\text{cs}} = -790V$

Of note in Figure 4 is the initial increase in separation distance before the control settles to the nominal value. This is because only two spheres are used in the charge structure. Table 1 indicates that two spheres placed symmetrically out of plane results in a fully controllable system, but this is due to the coupling in the Hill x- and y-directions. This is illustrated in Figure 6, which shows the offset from nominal for each of the Hill directions.

If the controller simply pulled the sphere in the along-track direction, some radial change would occur. Two spheres out of plane cannot generate an electric field to

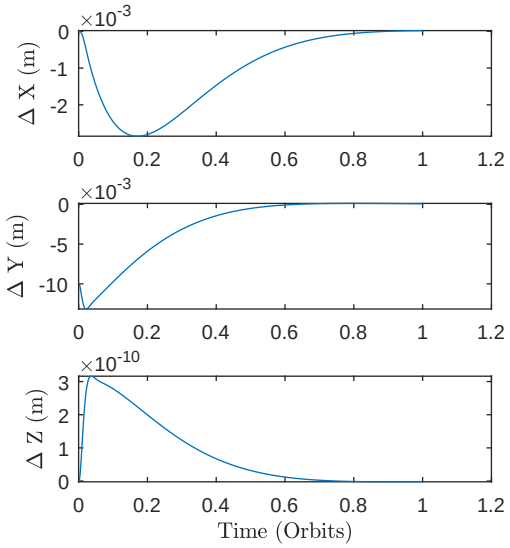

Fig. 6: Hill vector component differences

fully control in this direction. By leveraging the system dynamics, and specifically the known in-plane coupling exhibited by the HCW equations, the system is able to recover controllability.

While the simulation above demonstrates the effectiveness of the control given parameters that enhance controllability, the values in Table 2 and the assumptions state above do not fit a realistic mission scenario. The parameters in Table 3 are used in the simulation to follow. They are chosen to be commensurate with the dimensions of the leader shown in 4.

Table 3: Mission Scenario Design Parameters

Parameter	Value
V_{f}	1000V
n	3
r_{cs}	0.1m
r_{s}	0.1m

The size and mass of the leader craft were based roughly on the Iridium spacecraft to provide a reasonable baseline for a LEO mission. The follower is assumed to be a spherical craft small enough to fit within the wake of the leader. To simulate the effects of the wake on atmospheric drag, the drag coefficient of the follower is set to 0.

Table 4: System Physical Parameters

Parameter	Leader	Follower
Area (m^2)	0.5	0.008
Mass (kg)	1000	1
Coefficient of Reflectivity	1	1
Coefficient of Drag	2.2	0

The previous assumption that the follower position is known perfectly is relaxed. White Gaussian noise of $\sigma_r = 10^{-3}$m,$\sigma_v = 10^{-5}$m/s is added to the range value input to the controller. To account for this, the control is run at a lower frequency than the measurements are coming in. Ten range measurements are averaged while the control voltages are held constant.

Solar Radiation Pressure (SRP) is included as an unmodeled perturbation. Both drag and SRP vary as they pass in and out of sunlight. Drag is varied sinusoidally by $\pm 30\%$, while SRP is cut completely in shade. Finally, the same 1cm offset is introduced to start as was previously.

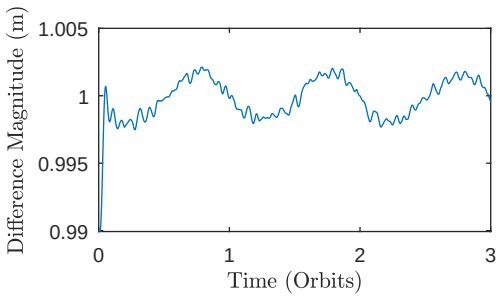

Fig. 7: Hill-frame follower position

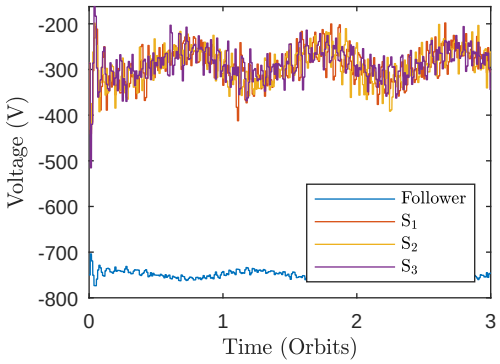

Fig. 8: Total system voltages

Figure 7 shows the control performance of the system. With unmodeled accelerations and noisy range measurements, the system still remains very near the nominal position. The ability of the control to remain exactly at this location is compromised, however it does stay within a 4mm bound — well within the sub-centimeter accuracy required by DCPA.

Figure 8 shows the total voltage sourced at a given timestep — note this is a difference from Figure 5, which showed the change in voltage from the nominal. Note that the "pusher-only" control described in previous sections is sufficient, as no positive voltages are sourced.

The drag, Coulomb, and SRP accelerations are shown for both the leader and follower in Figure 9. Two-body gravity is not included on this plot because it is many or-

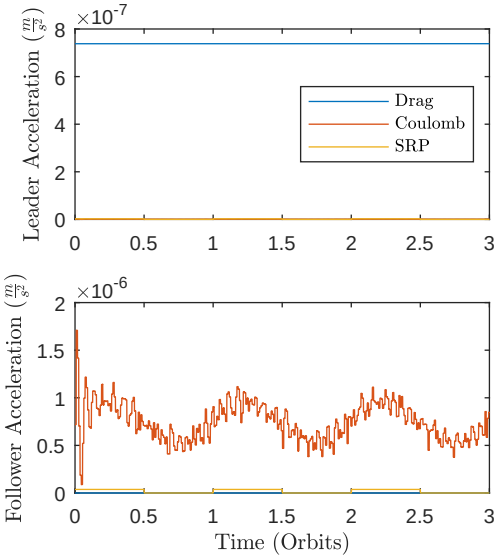

Fig. 9: Drag, Coulomb, and SRP acclerations on the leader and follower crafts

ders of magnitude larger. Note that the drag acceleration dominates for the leader craft. This is because the equal and opposite Coulomb force produces a much smaller acceleration due to the large mass of the leader. The follower Coulomb acceleration dominates over SRP, and is on roughly the same order as the drag acceleration as the leader. As it is generated based on knowledge of the nominal drag acceleration, this matches intuition. It is slightly larger than drag partially because it is correcting on noisy measurements, and also because it is also correcting on the discrepancy between the HCW linearization and true two-body dynamics.

6. Conclusion & Future Work

Coulomb actuation is applied to close-proximity leader-follwer formation with the goal of maintaining relative position with high precision. The DPCA mission concept is used to guide the generation of feasible parameters. A formulation of the Coulomb acceleration is provided using MSM, and is then linearized about the state and control variables for application to a linear controller. The nonlinear dynamics are also used to generate a minimum follower voltage for a given system geometry, which provides additional feasibility insight. Linear controllability is assessed on a system with the linearized Coulomb acceleration as well as linearized HCW and drag, and parameters are chosen to minimize the control norm. Simulations are performed with these and the system is shown to behave as expected. Finally, more mission-appropriate parameters and assumptions are used in a simulation which demonstrates that the controller still functions, though not as well as in the idealized case.

The linear controller used throughout is sensitive to gain selection. Each new set of parameters required new gains to be selected, some of which caused the follower voltage to drop below the allowable value shown in Eq. (16), or cause the dynamics to diverge, possibly because the system left the linear regime. A weakness of the controller is the various linearizations that are performed to derive it. HCW is linearized about small separations, drag about a given density, and the Coulomb acceleration about both the relative positions and voltages. The many benefits of a linear controller were reaped at the cost of significant effort matching parameters and gains. Nevertheless, the controller performed well when tuned correctly. Future iterations of this concept will investigate the application of nonlinear control techniques. Additionally, a physical model of the wake will be implemented to provide insight into power requirements and control authority under electrostatic shielding.

REFERENCES

[1] Gordon Roesler. Robotic Servicing of Geosynchronous Satellites (RSGS) Proposers Day Briefing prepared for Robotic Servicing of Geosynchronous Satellites (RSGS) Proposers Day. 2016.

[2] Niels H. Roth, Ben Risi, C. Cordell Grant, and Robert E. Zee. Flight Results from the CanX-4 and CanX-5 Formation Flying Mission. *4S Symposium*, (1):1–15, 2016.

[3] David A. Vallado. *Fundamentals of Astrodynamcs and Applications*. Space Technology Library, 4th edition, 2013.

[4] Cyrus Foster, Henry Hallam, and James Mason. Orbit determination and differential-drag control of Planet Labs cubesat constellations. *Advances in the Astronautical Sciences*, 156:645–657, 2016.

[5] Frank Marcos, Bruce Bowman, and Robert Sheehan. Accuracy of Earth's Thermospheric Neutral Density Models. *AIAA/AAS Astrodynamics Specialist Conference and Exhibit*, pages 1–20, 2006.

[6] Lb King and Gg Parker. Spacecraft formation-flying using inter-vehicle coulomb forces. *NASA Institute for . . .* , pages 1–103, 2002.

[7] Hanspeter Schaub, Gordon G Parker, Lyon B King, and Jan June. Challenges and Prospects of Coulomb Spacecraft Formation Control of the Astronautical Sciences Challenges and Prospects of Coulomb Spacecraft Formation Control. *Journal of the Astronautical Sciences*, 52:169–193, 2004.

[8] Arun Natarajan and Hanspeter Schaub. Linear dynamics and stability analysis of a Two-Craft Coulomb tether formation. *Advances in the Astronautical Sciences*, 120(II):1635–1649, 2005.

[9] Daan Stevenson and Hanspeter Schaub. Multi-Sphere Method for modeling spacecraft electrostatic forces and torques. *Advances in Space Research*, 51(1):10–20, 2013.

[10] D E Hastings. A review of plasma interactions with spacecraft in low Earth orbit. *Journal of Geophysical Research*, 100(A8):14457–14483, 1995.

[11] Benoit Durand de Gevigney, Thomas Sunn Pedersen, and Allen H Boozer. Debye screening and injection of positrons across the magnetic surfaces of a pure electron plasma in a stellarator. *Physics of Plasmas*, 18(1):013508, 2011.

[12] Elvis D. Silva. A Formulation of the Clohessy-Wiltshire Equations to Include Dynamic Atmospheric Drag. *AIAA/AAS Astrodynamics Specialist Conference*, (August), 2008.

[13] Andrew T. Harris, Christopher Petersen, and Hanspeter Schaub. Linear Coupled Attitude-Orbit Control Through Aerodynamic Forces. *2018 Space Flight Mechanics Meeting*, (January):1–13, 2018.

[14] Arun Natarajan, Hanspeter Schaub, Gordon G Parker, Arun Natarajan, Hanspeter Schaub, and Gordon G Parker. Reconfiguration of a Nadir-Pointing 2-Craft Coulomb Tether Journal of British Interplanetary Society. 60(6):209–218, 2007.